# Comparison of As Cast and T6 heat treatment on high end-of-life-scrap secondary aluminium alloy for High-Pressure Die Casting automotive structural components

A. Bongiovanni, A. Castellero, M. Da Silva

The automotive industry is working towards further reducing the carbon footprint of its vehicles and, with the electric vehicle transition, the raw materials used for the car itself need to be decarbonized. Aluminium alloys offer infinite recyclability, but they are sensitive to the Fe embrittlement that derives from recycling. High-pressure die casting AlSi10MnMg alloy is the most used alloy for structural components and is typically primary quality due to the high performances required. The present study investigates the behavior of structural secondary AlSi10MnMg alloy developed in the SALEMA European project. The alloy is designed at the upper tolerance level of EN 1706 43500 alloy with 70% and 90% end-of-life recycle content. This study analyzes the microstructure and casting defects, corrosion behavior and mechanical properties (bending and hardness tests) between as cast and T6 heat treatment. The microstructure and hardness are like the ones of primary alloys.

**KEYWORDS:** SECONDARY ALUMINIUM ALLOY, HIGH PRESSURE DIE CASTING, ALSI10MNMG, T6, HEAT TREATMENT, AUTOMOTIVE, STRUCTURAL

## INTRODUCTION

The European automotive industry has greatly reduced the carbon footprint of its fleet, passing from 159 $gCO_2$/km in 2007 to 96 $gCO_2$/km in 2021 [1]. The radical transition from Internal Combustion Engines (ICE) to Battery Electric Vehicles (BEV), has decreased even more the carbon footprint of the passenger cars. The next step is the decrease of the $CO_2$ emission of the raw materials used for manufacturing the vehicle itself. Aluminium represents a key contributor of this green transition, as it allows lightweighting and high recyclability. Many automotive components are already manufactured with secondary aluminium alloys, but most of them are applied for engine block, cylinder heads and in general components of ICE vehicles. Casting is the main manufacturing process involved in aluminium components production, representing 65% of the total aluminium weight in cars produced in 2019 [2]. Al-Si-Mg-based alloys are the most used in high-pressure die casting (HPDC) [3], with AlSi10MnMg alloy being one

A. Bongiovanni, A. Castellero
Department of Chemistry, NIS, University of Turin, Italy

M. Da Silva
Eurecat, Centre Tecnològic de Catalunya, Spain

andrea.bongiovanni@unito.it, manel.dasilva@eurecat.org, alberto.castellero@unito.it

of the first developed high-performance HPDC alloys. The aluminium used in the Body-In-White (BIW) has high mechanical requirements especially in elongation at fracture and yield strength, as it needs to absorb a large amount of energy during a crash and protect the passengers. These components are called structural, and the aluminum alloys involved in their manufacturing are primary, with low content of Fe especially. Fe is detrimental to ductility due to the intermetallics that forms when combined with Si, especially the acicular brittle β-$Al_5FeSi$ compounds. AlSi10MnMg alloy is designed to suppress this phase in favor of the less detrimental α-$Al_{15}(Fe,Mn)_3Si_2$ phase thanks to the addition of Mn. The aluminium is an infinitely recyclable material [4], but the recycle increases the content of detrimental elements such as Cu, Zn and especially Fe. This is the main reason for the scarce use of secondary alloys for structural components. In this work, two AlSi10MnMg structural HPDC alloys produced from end-of-life (EoL) scrap are studied. These alloys are designed and produced in the framework of the SALEMA European project [5] that try to apply the actual state-of-art of the secondary metallurgy to the alloys used for structural automotive components. The chemical composition used are compared and close to the EN 1706 international standard [6] that defines the ranges of each element for the EN 43500 alloy, standard name for AlSi10MnMg. In some chemical variants, the tramp elements exceed the standard limits for allowing higher recycled content. The work includes the most important tests required for validation in automotive: micrographic analysis of defects and microstructure, corrosion behavior, as it is a high-recycle secondary alloy and mechanical properties. The latter are assessed by means of a bending test, which evaluates the ductility, and hardness test for the strength.

## MATERIALS AND METHODS

In this work, two different alloys (Variant 4 and Variant 6) were chosen with different levels of EoL scrap recycled content (70% and 90%, respectively) among the six AlSi10MnMg variants developed in the SALEMA project. Variant 4 (V4) is the alloy with the minimum recycle and Fe content and Variant 6 (V6) is the alloy with the highest recycled content. As shown in Tab. 1, the two variants are designed at the high tolerances of the EN AC 1706 43500 alloy, with V6 exceeding the limits for Fe and Cu. The Sludge Factor (SF) is an empirical parameter that describes the tendency of the alloy to solidify and segregate intermetallics, typically α-$Al_x(Fe,Mn,Cr)_ySi_z$, prior to the formation of the dendrites in the holding furnace and/or the shot sleeve [7]. The SF is obtained usually by applying the Gobrecht [8] and Jorstad [9] empirical equation:

$$SF = (1 \times wt\%\ Fe) + (2 \times wt\%\ Mn) + (3 \times wt\%\ Cr) \quad (1)$$

**Tab.1** - Chemical composition measured by Optical Emission Spectroscopy (OES), Sludge Factor (SF) and recycle content (%).

| Alloy | Chemical composition [wt. %] | | | | | | | | | | Sludge Factor | Recycle % |
|---|---|---|---|---|---|---|---|---|---|---|---|---|
| | Si | Mg | Fe | Mn | Cu | Zn | Cr | Sr | Sr (ppm) | Al | | |
| EN 43500 | 9-11.5 | 0.15-0.6 | < 0.2 | 0.4-0.8 | < 0.03 | < 0.07 | < 0.03 | < 0.0025 | < 250 | bal. | 361,3 | 361,3 |
| Variant 4 | 10.48 | 0.14 | 0.17 | 0.58 | 0.02 | 0.01 | 0.01 | 0.020 | 200 | bal. | 336,9 | 336,9 |
| Variant 6 | 10.52 | 0.18 | 0.26 | 0.64 | 0.06 | 0.01 | 0.01 | 0.0133 | 133 | bal. | 342,6 | 342,6 |

A 5250-kN locking force Buhler cold chamber HPDC machine equipped with a VDS vacuum unit (V-HPDC), a shot sleeve with an internal diameter of 60 mm and a stroke of 450 mm was used for producing the specimens for the characterization. The die was designed to fabricate a 180x170 mm flat plate teste piece with 3 mm thickness at 100 mbar residual pressure, obtained by a ProVac CV 300 chill vent. The melt temperature during casting was 720°C, and the mold was heated by oil circulation to approximately 180°C. Part of the plates produced

underwent T6 heat treatment, including solution heat treatment at 490°C for one hour, water quenching and artificial ageing at 230°C for one hour. The T6 parameters were selected as the optimal set of time and temperature, following the results obtained in another task of the SALEMA project. The microstructure of the samples was examined using an optical microscope after etching for 10 seconds with a solution of 0.5 ml HF and 99.5 ml distilled $H_2O$. The cross section of the metallographic specimens was 30x3 $mm^2$. The bending tests were carried out on 50x50 mm samples with test parameters established based on VDA 238-100 standard [10]. A universal tensile machine equipped with a bending device was used for this test. This setup used a 0.2 mm radius. The hardness was measured on the surface of the casted plates using an EMTO-TEST DuraVision G5 Brinell machine. The evaluation of the corrosion behavior was performed following the B368 standard using uncoated plates. ASTM B368 is also known as CASS test (Copper-Accelerated Acetic Acid-Salt Spray (Fog)) and is a typical test used in the automotive field. For each condition (heat treatment and variant), rectangular 100x60 mm shape specimens were weighted before being put inside the corrosion chamber for 168h. At the end of the tests, the specimens were cleaned from the corrosion products, by dipping the specimens in a chloride acid bath, and then weighed to assess the weight loss. The specimens for the micrographic, bending and hardness test were cut out from the center of the casted plates. The corrosion specimen's location in the die has no influence on the corrosion behavior as they were cut out randomly from the plate. Three specimens per type were used in each test.

## RESULTS AND DISCUSSION

Given the similar results from the micrographic examination between Variant 4 (V4) and Variant 6 (V6), only V6 images will be shown in the present work, as more interesting from the recycle content point of view. The microstructural results and discussions will be considered representative for both alloys.

**Defects and microstructure analysis.** HPDC is a complex process due to the short cycle time and quick filling time involved. This combination makes HPDC a defect generating process [11], with porosity, cold flakes, cold joints and other casting defects. For this reason, it is important to include their assessment when studying new alloy, especially when it is with high recycled content. To evaluate the effect of T6 heat treatment, Fig. 1(b) shows how the porosity evolves from the as-cast (F) to the T6 state. The air entrapped naturally in the aluminum during the quick injection phase is a characteristic feature of the HPDC process and one of the major defects, as reported by Bonollo [11]. During the T6 high-temperature solution step, the air entrapped expands and can join with the surrounding air and so create bigger pores. It can be observed in Fig. 1b, where it is visually clear how T6 creates higher porosity. It is obvious how porosity is detrimental especially for ductility, as it decreases the cross section and acts as initiation point for fracture during elongation. There are two main types of pores: gas entrapment and shrinkage porosities. At this magnification level, the pores visible are due to trapped air since they show spherical shape, while the shrinkage pores can only be seen at higher magnification.

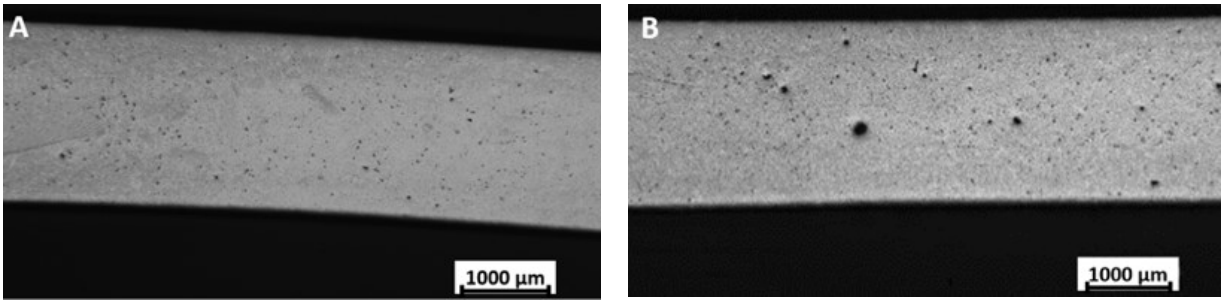


**Fig.1** - Optical micrographs showing the porosities in the F (a) and T6 samples (b).

Fig. 2(a) and Fig. 2(b) show cold flakes in the as-cast and heat treated (T6) samples, respectively. Cold flakes are casting defects that form during the injection of the liquid metal in the die cavity. During the filling time of the shot sleeve, a layer of aluminum first solidifies and oxidizes in the cold chamber and when the plunger injects the molten material in the die, the solidified layer is broken in many small particles around the casting [12]. The cold flake shows a different microstructure, evidenced in the inset of Fig. 2(a) and Fig. 2(b), that creates a discontinuity from the material solidified in the die. The microstructure of the cold flake shows very fine and blocky silicon eutectics, as shown in the inset of Fig. 2(a). The cold flake is not dissolved after T6 treatment as visible in Fig. 2(b), where the defect can be observed even at low magnification. The microstructure is unchanged even if the silicon eutectics are less dispersed and show the characteristic spheroidal shape obtained during solution treatment, as reported in the inset of Fig. 2(b).

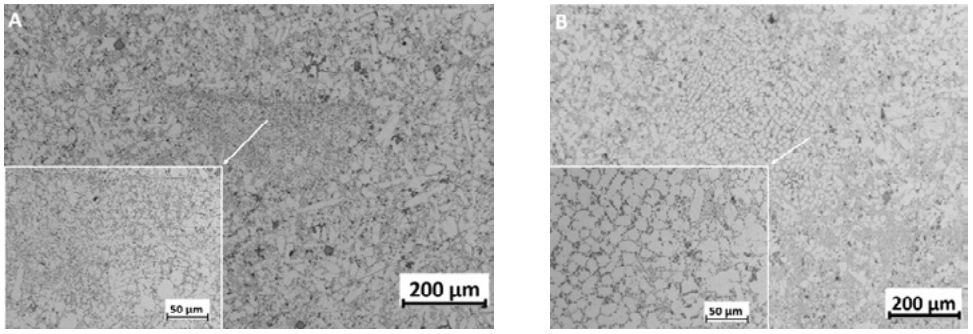


**Fig.2** - Cold flake in the F (a) and T6 (b) samples, insets show magnification of the defects microstructure.

Fig. 3 shows cold joints defects found in the plate sections. It can be observed how the microstructure is different at the two sides of the line of the cold joint. This happens when, during the filling of the die, a molten metal flow that has a superficial oxide layer meets another liquid front. The microstructure of the metallurgic interface, inset of Fig. 3(a), is characterized by very fine eutectic silicon, due to the higher solidification rate of the first layer, as happened for the cold flake. The T6 treatment homogenizes the microstructure, Fig. 3(b), losing the ultra-fine fibrous eutectics, but highlighting the microstructural discontinuity due to the interface. In fact, the air entrapped between the superficial oxide layers during the matching of the two flows expands and creates a void during the heat treatment cycle. In Fig. 3(b) it can be noted how the microstructure changes at the sides of the cold joint, as a result of the different cooling rate and the two flows.

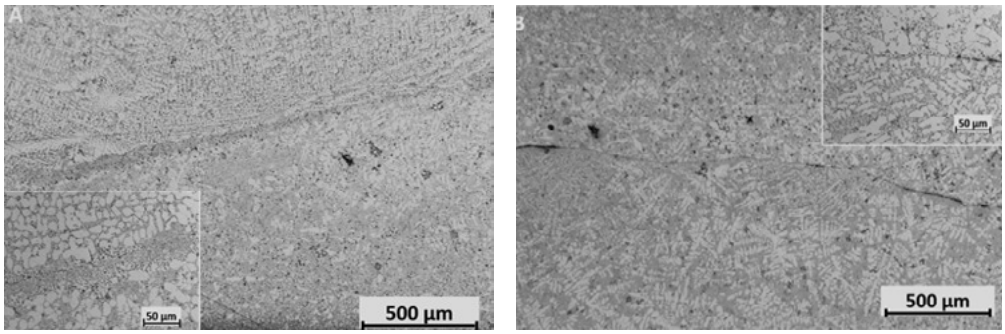


**Fig.3** - Cold joint in the F (a) and T6 (b) samples, insets show magnification of the defects microstructure.

Given the low amount of Fe and the high Mn content, as shown in Tab. 1, together with the low thickness and corresponding high cooling rate, very few β- $Al_5FeSi$ needle shape intermetallic compounds were found in the samples. Considering the chemical composition, it was expected to be much more present the α-$Al_{15}(Fe,Mn)_3Si_2$ phase. The Fe/Mn ratio was selected for suppressing the brittle acicular β phase, while promoting the α compound, as explained also by Taylor [13]. The α-AlSiMnFe has a Chinese script-like shape as shown in Fig. 4 and they can be divided in primary and secondary, i.e., α1- AlSiMnFe and α2- AlSiMnFe, respectively. Primary α are coarse and solidifies in the shot sleeve or during the transfer from the cold chamber to the shot sleeve [14]. Secondary α intermetallics instead forms in the die cavity during the solidification and show a more equiaxial morphology. α1-AlSiMnFe are characterized by bigger dimension with a Feret diameter around 30-50 μm, while α2-AlSiMnFe are much finer with a Feret diameter one order of magnitude smaller, in the order of the units of μm. This different dimension and microstructure were also found by Bosch et al. [3] with a secondary alloy having similar chemical composition. Neither the coarse nor fine α phase dissolve or change shape and dimension during T6 treatment, as can be seen by comparing Fig. 4(a) and Fig. 4(b). The strontium chemical modification led to the absence of acicular eutectic Si even in the as cast state [14], in favor of a more fibrous morphology, Fig. 4(a). After T6 and solution treatment, Fig. 4(b), the eutectic Si is transformed into spherical form with a less detrimental and brittle shape. This is the microstructural goal of an effective T6 treatment that results in an enhancement of the ductility of the component.

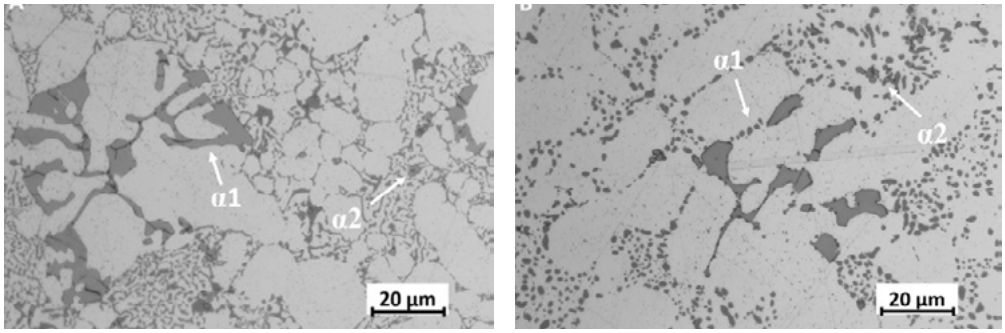


**Fig.4** - Microstructure and α1- AlSiMnFe and α2- AlSiMnFe intermetallics in the F (a) and T6 (b) samples.

**Corrosion behavior.** The effect of the corrosive chamber, that simulates an accelerated salty fog environment, on the uncoated aluminum is shown in Tab. 2 in terms of weight loss. There is a clear trend difference between the F and T6 state, while only a slight variation between V4 and V6. The higher-recycle content alloy (V6) showed worse corrosive behavior, and this could be due to the higher Fe content that leads to increased Fe-rich intermetallics content that are known to have higher corrosion-susceptibility [15]. The T6 heat treatment is performed at high temperature in a non-inert atmosphere and so the hypothesis is that an oxidation passive layer grows on the surface that protects the plates from the corrosive environment. During the micrographic analysis, no evidence of this layer was observed. The hypothesis is that the oxide layer is thinner than a micron, but it is enough to protect the aluminium substrate by an accelerated yet non extreme corrosive environment as the CASS test. Further analysis is needed to assess this different behavior, using more powerful techniques like XPS and AFM, as a scanning electron microscope (SEM) could not be powerful enough.

**Tab.2** - Weight and weight losses (in grams and percentage) of the uncoated specimens after the 168h CASS test.

| Alloy | Heat Treatment | Initial Weight | Weight after 168 h CASS | Weight loss | |
|---|---|---|---|---|---|
| | | | | (g) | % |
| V4 | F | 122.2 | 113.2 | 9.0 | 7.4 |
| V6 | | 119.6 | 109.0 | 10.6 | 8.8 |
| V4 | T6 | 120.5 | 119.3 | 1.2 | 1.0 |
| V6 | | 116.5 | 114.3 | 2.2 | 1.9 |

**Mechanical properties.** Bending test results correlate with the elongation at fracture as it assesses the ductility of the alloy, while hardness is related to the yield strength and ultimate tensile strength. Tab. 3 reports the bending angles and can be firstly noted the increment in ductility after T6. It is interesting to point out how also the standard deviation of the result decreases after the heat treatment, since it acts as a homogenization treatment. Very slight differences can be noted between the chemical variants in the as-cast state, while some differences can be appreciated after T6. V4 shows higher ductility than V6, even if the starting point at F state is close. The V6 has in fact more Fe as shown in Tab. 1 that leads to larger amounts of intermetallic, that even in the α form, leads to lower ductility. This slight difference in chemical composition also results in a lower standard deviation for V4 in both F and T6 states with respect to V6. The higher Fe can increase the porosity [13] in the material and the higher presence of Mn allows the formation of more α1 intermetallic particles or sludges.

**Tab.3** - Mechanical properties: bending angle with standard deviation and Brinell hardness results.

| Alloy | Heat Treatment | Bending VDA 238-100 | | Hardness Brinell | |
|---|---|---|---|---|---|
| | | average | st.dv | average | st.dv |
| V4 | F | 22.3 | 7.0 | 85.3 | 1.6 |
| | T6 | 58.5 | 0.6 | 67.5 | 1.0 |
| V6 | F | 23.1 | 9.9 | 82.2 | 2.9 |
| | T6 | 51.4 | 1.9 | 76.0 | 1.5 |

Given the numerous casting and solidification defects as the ones presented previously, bending test can give more reliable data than a traditional tensile test. The resistant section is less sensitive to the defects, since only half of it is under tension, and the skin-effect of the component, characterized by a finer microstructure, improves the mechanical performance. Tab. 3 reports the averages of the hardness measurements. The effect of the T6 decreases the hardness in both alloys, but V6 keeps a higher hardness than V4. This result agrees with the bending angle. The higher Fe content of V6 increases the hardness and tensile strength of the alloy, in agreement with Li [16]. The values obtained for both alloy variants satisfy the minimum hardness values specified by the EN 1706 standard, i.e., 80 HB for F temper and 65 HB for T6 [6].

## CONCLUSIONS

In the present study, two variants of high-performance AlSi10MnMg aluminum alloy produced with high end-of-life scrap recycle content has been characterized. Microstructural analysis, corrosion test, bending and hardness test were performed in the as cast and T6 conditions.

- The chemical composition of the two alloys differs mainly for the Fe and Cu content that derives from the higher recycle rate of V6 and the Mn content to counterbalance the Fe level.
- Despite the very high recycled content of the alloy, the detrimental element (mainly Fe, Cu and Zn) has been kept close to the reference standard EN 1706 upper limit, with V6 exceeding the Fe and Cu limit.
- The microstructure does not differ between the two

alloys, with the same casting and solidification defects and intermetallic compound. The T6 treatment has the same effect on microstructure. Few brittle β phases are formed in the alloy.

- The corrosion resistance is largely affected by the T6 treatment that is believed to have created a passivation oxide layer that greatly reduced the corrosion during CASS test. The higher Fe content of V6 leads to slightly higher corrosion susceptibility due to higher Fe intermetallics.
- The mechanical properties, measured with bending and hardness test, change after the heat treatment between the variants, while in the as cast state show similar values. The ductility of V6 after T6 decreases with respect to V4, probably as a consequence of the increased Fe content.
- The mechanical properties (hardness) of the samples obtained using EoL secondary alloys satisfy the requirements fixed for the primary alloy.

In perspective, the investigation of these alloys will continue for understanding the improved corrosion resistance, the effect of T5 heat treatment and the correlation of the mechanical properties to the presence of Fe intermetallics.

## ACKNOWLEDGEMENT

The results presented in this work have been partially obtained within the framework of project Horizon 2020 SALEMA, Grant Agreement no. 101003785.
The author would like to thank CRF Centro Ricerche Fiat – Stellantis, partner of the SALEMA project, for the laboratory support and the permission to publish the results.
Authors from Università di Torino acknowledge support from the Project CH4.0 under the MUR program "Dipartimenti di Eccellenza 2023-2027" (CUP: D13C22003520001).

## REFERENCES

[1] ] Paltsev, Sergey & Chen, Y.-H. Henry & Karplus, Valerie & Kishimoto, Paul & Reilly, John & Loeschel, Andreas & von Graevenitz, Kathrine & Koesler, Simon, (2015). "Reducing CO2 from cars in the European Union: Emission standards or emission trading?", CAWM Discussion Papers 84, University of Münster, Münster Center for Economic Policy (MEP).
[2] Aluminum content in European Passenger Cars, Public Summary, 2019, Ducker Frontier.
[3] Bösch, Dominik & Pogatscher, Stefan & Hummel, Marc & Fragner, Werner & Uggowitzer, Peter & Göken, Mathias & Höppel, H.W. (2014). Secondary Al-Si-Mg High-pressure Die Casting Alloys with Enhanced Ductility. Metall and Mat Trans A. 46.
[4] Raabe, D.; Ponge, D. Making sustainable aluminum by recycling scrap: The science of "dirty" alloys. Prog. Mater. Sci. 2022, 128, 100947.
[5] https://salemaproject.eu/
[6] ISO 1706:2020, "Aluminum and aluminum alloys – Castings – Chemical composition and mechanical properties", Int. Organ. Stand, 2020.
[7] Ceschini, Lorella & Morri, Alessandro & Toschi, Stefania & Bjurenstedt, Anton & Seifeddine, Salem. (2018). Influence of Sludge Particles on the Fatigue Behavior of Al-Si-Cu Secondary Aluminium Casting Alloys. Metals. 8. 268.
[8] Gobrecht, J. Settling-out of Fe, Mn and Cr in Al-Si casting alloys. Giesserei 1975, 62, 263–266. 15.
[9] Jorstad, J. Understanding sludge. Die Cast. Eng. 1986, 30, 30–36
[10] VDA 238-100 test specification draft: Plate bending test for metallic materials. 12/2010
[11] Bonollo, F., Gramegna, N. & Timelli, G. High-Pressure Die-Casting: Contradictions and Challenges. JOM 67, 901–908 (2015).
[12] Ahamed, Aziz & Kato, Hiroshi. (2008). Effect of cold flakes on mechanical properties of aluminium alloy die casts. International Journal of Cast Metals Research - INT J CAST METALS RES. 21. 162-167.
[13] Taylor, John. (2012). Iron-Containing Intermetallic Phases in Al-Si Based Casting Alloys. Procedia Materials Science. 1. 19–33.
[14] A.K. Dahle, K. Nogita, S.D. McDonald, C. Dinnis, L. Lu, Eutectic modification and microstructure development in Al–Si Alloys, Mater. Sci. Eng.: A 413–414 (2005) 243–248.
[15] Bjurenstedt, Anton & Casari, Daniele & Seifeddine, Salem & Mathiesen, Ragnvald & Dahle, A. (2017). In-situ study of morphology and growth of primary α-Al(FeMnCr)Si intermetallics in an Al-Si alloy. Acta Materialia. 130.
[16] Zaidao Li, Nathalie Limodin, Amina Tandjaoui, Philippe Quaegebeur, Pierre Osmond, David Balloy, Influence of Sr, Fe and Mn content and casting process on the microstructures and mechanical properties of AlSi7Cu3 alloy, Materials Science and Engineering: A, Volume 689, 2017, Pages 286-297

TORNA ALL'INDICE >